Neuron

A Functional Non-coding RNA Is Produced from *xbp-1* mRNA

Graphical Abstract

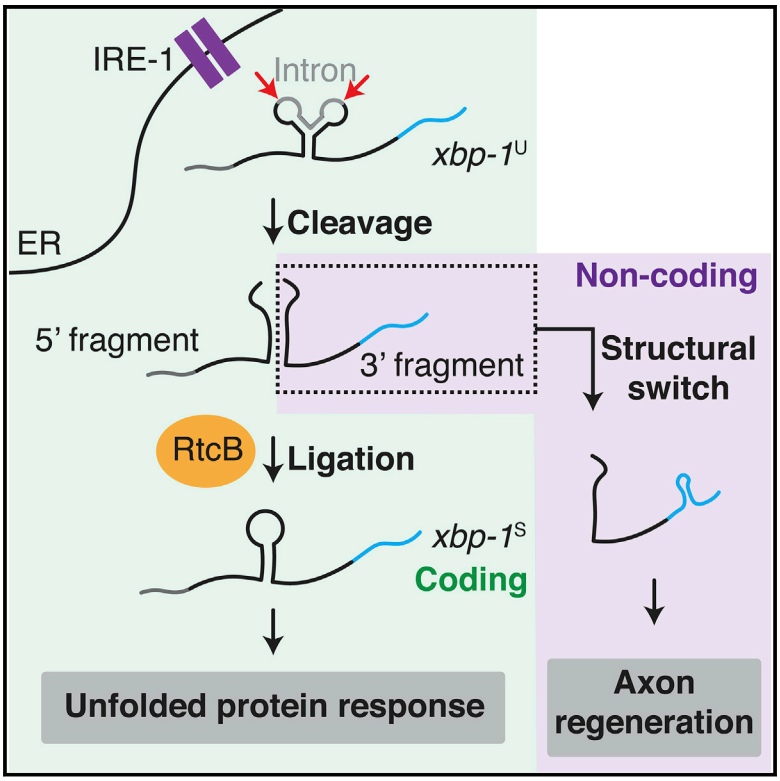

Authors

Xiao Liu, Jean-Denis Beaudoin, Carrie Ann Davison, Sara G. Kosmaczewski, Benjamin I. Meyer, Antonio J. Giraldez, Marc Hammarlund

Correspondence

marc.hammarlund@yale.edu

In Brief

Liu et al. show that the mRNA encoding the XBP-1 transcription factor has an unexpected second function in *C. elegans*. Cytoplasmic cleavage of *xbp-1* mRNA activates a ncRNA sequestered within the mRNA. This ncRNA is critical for axon regeneration and acts independently of the protein-coding function of the *xbp-1* mRNA.

Highlights

- Cytoplasmic cleavage of the *xbp-1* mRNA produces a biologically active ncRNA
- The *xbp-1* ncRNA affects neuronal regeneration and animal lifespan *in vivo*
- The function of the *xbp-1* ncRNA requires formation of an RNA stem
- The *xbp-1* ncRNA represents an XBP-UPR-independent output of the *xbp-1* locus

Liu et al., 2020, Neuron *107*, 854–863
September 9, 2020
https://doi.org/10.1016/j.neuron.2020.06.015

CellPress

CellPress

Neuron

Report

A Functional Non-coding RNA Is Produced from *xbp-1* mRNA

Xiao Liu,[1] Jean-Denis Beaudoin,[1] Carrie Ann Davison,[1] Sara G. Kosmaczewski,[1] Benjamin I. Meyer,[1] Antonio J. Giraldez,[1,2] and Marc Hammarlund[1,3,4,*]

[1]Department of Genetics, Yale University School of Medicine, New Haven, CT 06510, USA
[2]Yale Stem Cell Center, Yale University School of Medicine, New Haven, CT 06510, USA
[3]Department of Neuroscience, Yale University School of Medicine, New Haven, CT 06510, USA
[4]Lead Contact
*Correspondence: marc.hammarlund@yale.edu
https://doi.org/10.1016/j.neuron.2020.06.015

SUMMARY

The *xbp-1* mRNA encodes the XBP-1 transcription factor, a critical part of the unfolded protein response. Here we report that an RNA fragment produced from *xbp-1* mRNA cleavage is a biologically active non-coding RNA (ncRNA) essential for axon regeneration in *Caenorhabditis elegans*. We show that the *xbp-1* ncRNA acts independently of the protein-coding function of the *xbp-1* transcript as part of a dual output *xbp-1* mRNA stress response axis. Structural analysis indicates that the function of the *xbp-1* ncRNA depends on a single RNA stem; this stem forms only in the cleaved *xbp-1* ncRNA fragment. Disruption of this stem abolishes the non-coding, but not the coding, function of the endogenous *xbp-1* transcript. Thus, cleavage of the *xbp-1* mRNA bifurcates it into a coding and a non-coding pathway; modulation of the two pathways may allow neurons to fine-tune their response to injury and other stresses.

INTRODUCTION

The IRE1/XBP1 branch of the unfolded protein response (XBP-UPR) is conserved from yeast to human and is a critical component of the cellular response to protein stress in the endoplasmic reticulum (ER) (Walter and Ron, 2011). The output of the XBP-UPR is activity of the XBP-1 protein, a DNA-binding transcription factor encoded by the *xbp-1* locus. Translation of active XBP-1 protein requires processing of *xbp-1* mRNA by a non-canonical cytoplasmic RNA splicing event. This splicing event removes a short central sequence from the *xbp-1* mRNA, resulting in a frameshift that brings the functional C-terminal half of the XBP-1 protein into frame. Mechanistically, cytoplasmic *xbp-1*^{U} mRNA is first cleaved twice by the endonuclease IRE-1 (Calfon et al., 2002; Kawahara et al., 1998; Sidrauski and Walter, 1997; Yoshida et al., 2001). Next, the 5′ and 3′ fragments are ligated by the RNA ligase RtcB to generate the spliced *xbp-1*^{S} mRNA that encodes the XBP-1 protein (Figure 1A; Jurkin et al., 2014; Kosmaczewski et al., 2014; Lu et al., 2014; Sidrauski et al., 1996). The XBP-UPR is crucial for cellular protein homeostasis, and dysregulation of *xbp-1* splicing is implicated in inflammatory diseases, metabolic diseases, and several types of cancer (Jiang et al., 2015). In the nervous system, the function of the XBP-UPR has been associated with a wide range of neurodegenerative diseases, including Alzheimer's disease, amyotrophic lateral sclerosis (ALS), Huntington's disease, and Parkinson's disease (Hetz and Mollereau, 2014; Jiang et al., 2015).

We found previously that RtcB, the RNA ligase that is required for *xbp-1* splicing and the XBP-UPR, has a very strong effect on axon regeneration in *C. elegans* neurons. Neurons can respond to axon injury by initiating axon regeneration to restore structure and function. An unbiased functional screen (Nix et al., 2014) and detailed genetic analysis (Kosmaczewski et al., 2015) indicated that RtcB mutants have extremely high regeneration, among the strongest effects seen. This result was surprising because neuronal injury is a form of cellular stress, and RtcB mutants completely lack the XBP-UPR and die quickly when treated with tunicamycin to disrupt ER protein homeostasis (Kosmaczewski et al., 2014). Further experiments showed that the effect of RtcB required its ligase activity but was independent of the XBP-UPR. It was also independent of the ligation of tRNAs, the other RNA substrate of RtcB (Kosmaczewski et al., 2015). These data indicate that RtcB affects axon regeneration by an unknown mechanism involving RNA ligation.

Here we show that the *xbp-1* locus, in addition to encoding the XBP-1 protein, also encodes a biologically active non-coding RNA (ncRNA). The *xbp-1* ncRNA is the 3′ fragment produced by cleavage of the cytoplasmic *xbp-1*^{U} mRNA. The effect of RtcB on axon regeneration is in large part due to modulation of the *xbp-1* ncRNA function rather than the canonical output of the XBP-1 protein. We show that the function of the *xbp-1* ncRNA is context dependent and that it is not functional before cleavage, when it is still part of the *xbp-1*^{U} mRNA. We identify a rearrangement of secondary structure that correlates with *xbp-1* ncRNA activity and show that a single base pair within this structure is essential for ncRNA function.

ncRNAs are produced from various origins and biogenesis pathways. In addition to being generated from distinct regions

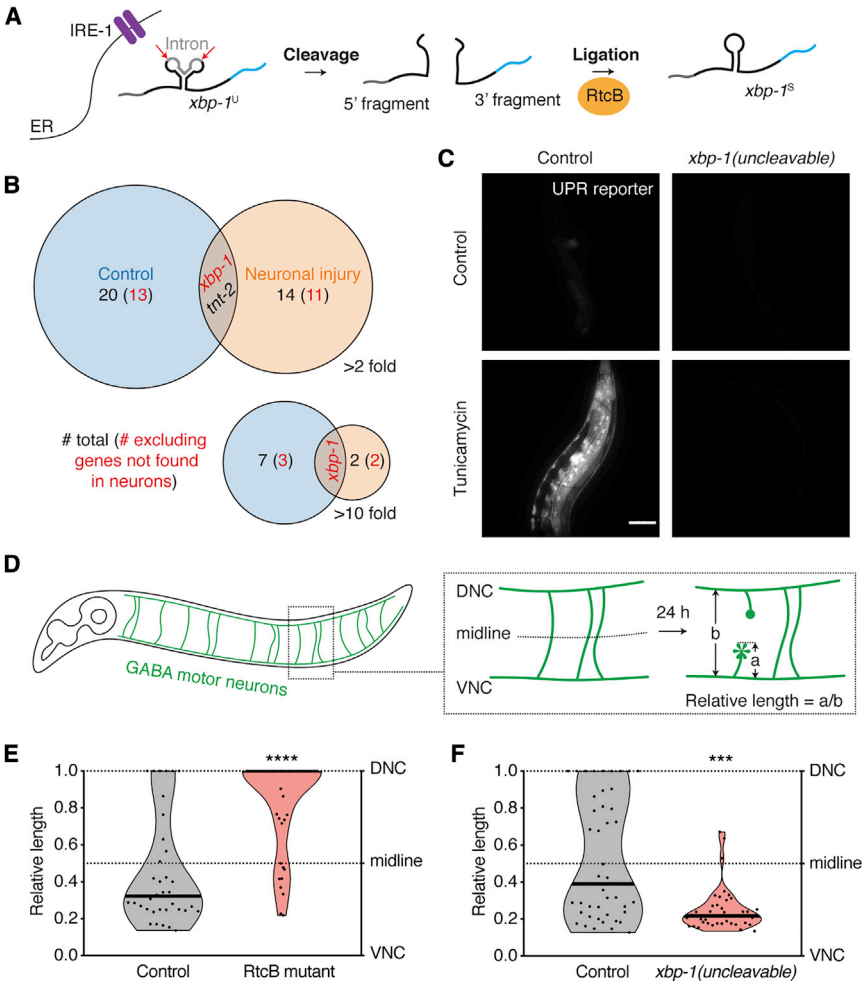

Figure 1. A Processing Intermediate of the *xbp-1* mRNA Promotes Axon Regeneration

(A) Diagram of the *xbp-1* mRNA splicing pathway.

(B) RNA-seq analysis identifies non-canonical RNA junctions that are enriched in RtcB mutant animals compared with non mutant controls. The Venn diagram plots genes with such RtcB-dependent junctions identified under normal conditions (blue) or with neuronal injury (orange) at the indicated fold change cutoff. See also Tables S1 and S2.

(C) Animals with uncleavable *xbp-1* fail to mount the UPR under control conditions or upon tunicamycin treatment (5 μg/mL, 24 h). Scale bar, 50 μm.

(D) Scheme of axotomy in *C. elegans* GABA neurons. DNC, dorsal nerve cord; VNC, ventral nerve cord.

(E) Animals deficient in the RNA ligase RtcB show significantly higher regeneration. n = 37 and 44 from left to right.

(F) Axon regeneration is eliminated in animals with the *xbp-1(uncleavable)* allele (see Figure S1 for details regarding this allele). n = 44 and 43 from left to right.

In (E) and (F), a black bar represents the median. ***p < 0.001, ****p < 0.0001, 2-tailed Kolmogorov-Smirnov (K-S) test.

from coding RNAs, ncRNAs can also be transcribed from genomic regions that are closely linked to coding genes. For example, many microRNAs (miRNAs) and circular RNAs (circRNAs) are processed from intronic regions of pre-mRNAs (Fu, 2014). However, it is less clear whether ncRNAs can be produced from functional, mature mRNAs. Only until recently has it been postulated that coding RNAs can also have non-coding functions (Crerar et al., 2019; Kumari and Sampath, 2015; Sampath and Ephrussi, 2016). By characterizing the non-coding function of the *xbp-1* locus, our study provides the first example of a ncRNA directly derived from the cleavage of a mature mRNA. Discovery of a ncRNA pathway that coexists with the coding function of the *xbp-1* locus opens a new window into the molecular mechanisms neurons use to respond to cellular conditions.

RESULTS

Blocking *xbp-1* mRNA Cleavage versus Ligation Results in Opposite Phenotypes in Axon Regeneration

RtcB mutant animals, which completely lack the XBP-UPR because the *xbp-1* RNA fragments cannot be ligated to produce the protein-coding *xbp-1*^{S}, have extremely high axon regeneration (Kosmaczewski et al., 2015). However, the high regeneration phenotype in these mutants is not caused by loss of the XBP-UPR because inactivating or activating the XBP-UPR does not phenocopy or rescue RtcB mutants and, overall, has relatively minor effects on regeneration (Kosmaczewski et al., 2015). The high regeneration phenotype is also not due to lack of tRNA maturation, despite the clear role of RtcB in ligating tRNAs (Englert et al., 2011; Popow et al., 2011; Tanaka and Shuman, 2011).

We considered the possibility that an unidentified RNA substrate mediates the effect of RtcB ligation on axon regeneration. We performed RNA sequencing (RNA-seq), comparing RtcB mutant animals and non mutant controls, and searched for RtcB-dependent RNA junctions that did not have the canonical sequences used by the spliceosome (STAR Methods). To account for the possibility that neuron stress was required, we sequenced both groups with and without neuronal injury, using a mutation in β-spectrin (*unc-70*) to trigger spontaneous axon breaks (Hammarlund et al., 2007). The analysis (Table S1) confirmed that RtcB is required for production of the *xbp-1*^{S} mRNA because the RtcB-dependent junction was more than 500-fold enriched in the presence of RtcB compared with RtcB mutant animals. Further, this enrichment was observed under normal conditions and in the β-spectrin mutant background, suggesting that *xbp-1* splicing occurs constitutively and is not altered significantly by neuronal injury. However, when comparing all junctions using a fold change cutoff of 10, we identified only 3 genes when we compared the two groups with neuronal injury and 8 genes when without. Other than *xbp-1*,

there was no overlap between the two sets of genes (Figure 1B; Table S2). The effect of RtcB on axon regeneration is neuron autonomous (Kosmaczewski et al., 2015), but many of the genes we identified are not expressed in neurons (Figure 1B; Table S2). Further, many of these junctions were located in non-coding regions near the 5′ or 3′ ends of transcripts and likely have little effect on gene function (Table S2). Overall, we did not identify strong candidates other than *xbp-1* for RtcB-mediated ligation.

Thus, we considered the possibility that another function of the *xbp-1* gene, independent of the XBP-UPR, might affect axon regeneration. To better characterize *xbp-1* function, we sought to block *xbp-1*^{U} mRNA processing at the cleavage step rather than at the ligation step (as in the RtcB mutants). Cleavage of *xbp-1*^{U} mRNA is mediated by the IRE-1 endonuclease. However, IRE-1 has many RNA targets (Hollien and Weissman, 2006; Hollien et al., 2009). Further, unlike *xbp-1* mutants, *ire-1* mutant animals are visibly sick. These data suggest that IRE-1's additional targets are biologically important and might confound study of the XBP-UPR. Therefore, to specifically block the cleavage of *xbp-1*^{U} mRNA, we used CRISPR techniques to generate a novel allele, *xbp-1(uncleavable)* (Figure S1A). Cleavage of the *xbp-1*^{U} mRNA by IRE-1 requires a conserved RNA motif at the two cleavage sites (Gonzalez et al., 1999). We introduced mutations into the endogenous *xbp-1* locus that alter these motifs but do not affect amino acid coding in the *xbp-1*^{U} or the *xbp-1*^{S} frame (Figure S1B).

Cleavage and ligation are required for production of the *xbp-1*^{S} transcript that encodes the XBP-1 protein (Figure 1A). Consistent with this, *xbp-1(uncleavable)* animals could neither produce *xbp-1*^{S} (Figure S1C) nor activate the XBP-UPR (Figure 1C), similar to RtcB ligase mutants (Kosmaczewski et al., 2014). Interestingly, however, we found that these two mutants have completely opposite phenotypes in axon regeneration. RtcB ligase mutants have extremely high axon regeneration (Figures 1D and 1E), whereas the *xbp-1(uncleavable)* allele eliminates regeneration (Figure 1F). These data suggest that an *xbp-1* mRNA processing intermediate between the cleavage step and the ligation step functions in axon regeneration.

The *xbp-1* 3′ Fragment Promotes Axon Regeneration Independently of the UPR

During *xbp-1*^{U} mRNA processing, IRE-1 cleaves the mRNA twice, generating three fragments: a 5′ fragment, a central fragment, and a 3′ fragment. The 5′ and 3′ fragments are then ligated by RtcB to generate *xbp-1*^{S} mRNA. Blocking cleavage would be expected to result in depletion of all three fragments, whereas blocking ligation would be expected to cause relative accumulation of the 5′ and 3′ fragments. Thus, the opposite regeneration phenotypes in the cleavage and ligation mutants could be due to a novel function of these intermediate fragments. To determine which intermediate fragment is responsible, we generated *rtcb-1; xbp-1(zc12)* double-mutant animals. We found that this allele of *xbp-1*, which contains an early stop codon, suppresses the high regeneration phenotype in RtcB mutant animals (Figure 2A, control), likely because nonsense-mediated decay reduces overall *xbp-1* mRNA abundance, affecting all outputs of the *xbp-1* locus. We expressed transgenic *xbp-1* in this double-mutant background with the expectation that expressing the form of *xbp-1* that mediates regeneration would result in the *rtcb-1* phenotype of high regeneration. Expressing the *xbp-1* coding sequence along with its native 3′ UTR, either under its native promoter or under a gamma aminobutyric acid (GABA)ergic neuron-specific promoter, restored regeneration to the high *rtcb-1* single-mutant level. These data confirm that the function of the *xbp-1* locus in axon regeneration is cell autonomous, consistent with previous results from RtcB (Kosmaczewski et al., 2015), and indicate that the function of the *xbp-1* locus is mediated by some aspect of the *xbp-1* mRNA. However, when the endogenous *xbp-1* 3′ UTR was swapped with the commonly used *unc-54* 3′ UTR, expression of *xbp-1* was no longer able to restore regeneration (Figure 2A). These data indicate that the *xbp-1* 3′ UTR is required to promote axon regeneration in the *rtcb-1; xbp-1(zc12)* context. We concluded that the *xbp-1* 3′ fragment, which contains the 3′ UTR, is likely responsible for the high regeneration phenotype in the RtcB ligase mutant animals. In support of this, we detected, by northern blot, an accumulation of *xbp-1* 3′ fragments *in vivo* in RtcB mutant animals compared with controls (Figure 2B).

To further test the function of the *xbp-1* 3′ fragment and to determine whether it can promote axon regeneration outside of the RtcB mutant context, we overexpressed the 3′ fragment specifically in GABA neurons in a non-mutant background. We found that 3′ fragment overexpression increased axon regeneration (Figures 2C and 2E). To further characterize this effect in relation to the XBP-UPR, we used CRISPR techniques to completely delete the endogenous *xbp-1* gene. These *xbp-1(deletion)* animals had decreased regeneration (Figures 2D and 2E), similar to *xbp-1(uncleavable)* (Figure 1F). In this *xbp-1(deletion)* background, we expressed the *xbp-1* 3′ fragment specifically in GABA neurons. We found that 3′ fragment overexpression restored regeneration to normal levels (Figures 2D and 2E). Thus, overexpression of the *xbp-1* 3′ fragment is sufficient to increase regeneration in animals with a normal XBP-UPR and also in animals that completely lack conventional *xbp-1* transcripts and have no XBP-UPR. Further, preventing production of endogenous *xbp-1* 3′ fragments in *xbp-1(uncleavable)* (Figure 1F) and *xbp-1(deletion)* (Figure 2D) reduces regeneration below control levels, and this is rescued by expression of the 3′ fragment (Figure 2D). These data indicate that the *xbp-1* 3′ fragment is a critical part of the endogenous regeneration response.

The *xbp-1* 3′ Fragment Functions as a ncRNA

The *xbp-1* 3′ fragment contains some of the *xbp-1* coding sequence (Figure S2A), and the overexpression experiments (Figures 2C and 2D) included a start codon in the plasmid at the beginning of the *xbp-1* 3′ fragment sequence. We wanted to find out whether the *xbp-1* 3′ fragment acts as a ncRNA molecule or whether it encodes a functional peptide. We generated an *xbp-1* 3′ fragment construct with the plasmid start codon frameshifted (Figure S2A) and found that this construct retained its ability to promote regeneration (Figures S2B and 2C), suggesting that the coding potential of the *xbp-1* 3′ fragment is dispensable for function in regeneration. Next we attached only the predicted non-coding (UTR) portion of the *xbp-1* 3′ fragment to the GFP coding sequence, after the GFP stop codon, and expressed this construct (GFP-UTR) specifically in GABA neurons.

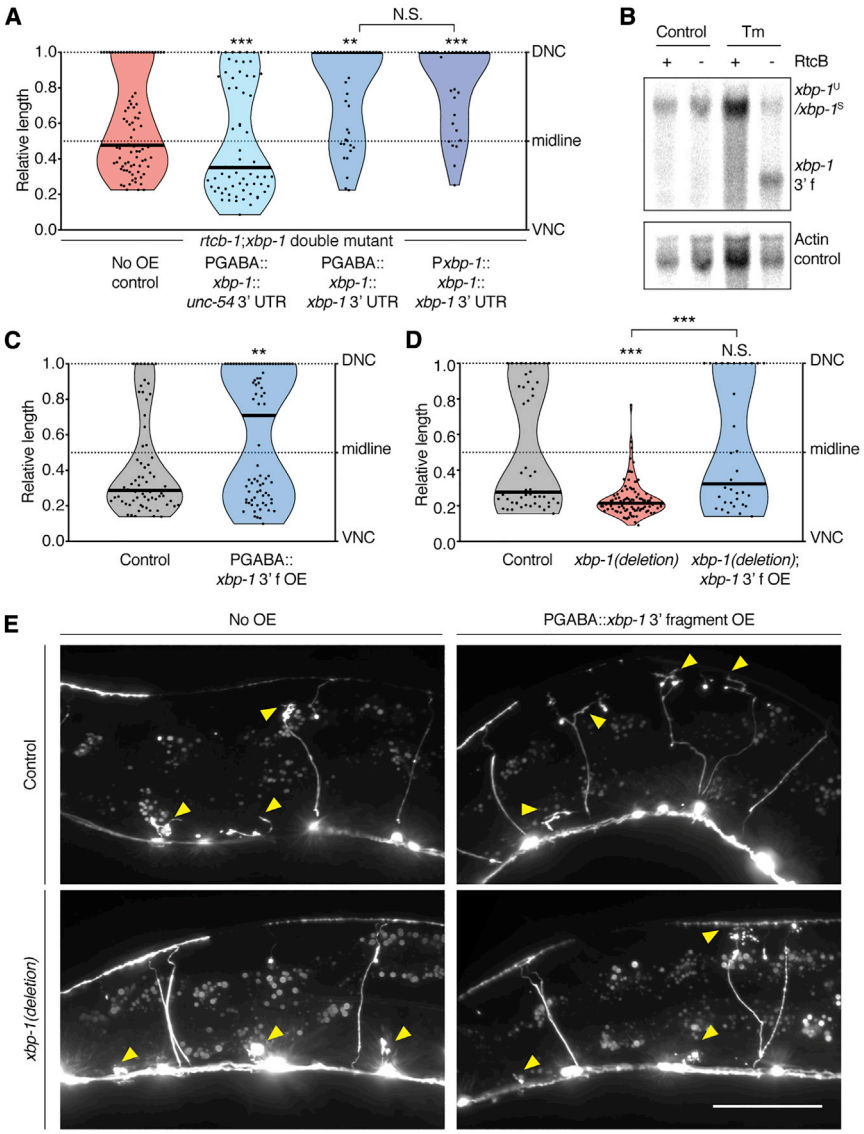

Figure 2. The *xbp-1* 3′ Fragment Is Necessary and Sufficient to Promote Axon Regeneration

(A) The *xbp-1* 3′ UTR is required to increase regeneration in the *rtcb-1(gk451); xbp-1(zc12)* double-mutant background. n = 62, 69, 40, and 31 from left to right.

(B) Northern blot showing *xbp-1* 3′ fragment accumulation in RtcB mutant animals.

(C) The *xbp-1* 3′ fragment is sufficient to increase regeneration cell autonomously. n = 70 and 79 from left to right.

(D) Deletion of the genomic *xbp-1* locus eliminates regeneration, which is rescued by GABA-specific expression of the *xbp-1* 3′ fragment. n = 52, 92, and 34 from left to right.

(E) Representative micrographs of animals of the indicated genotype 24 h after axotomy. Arrows indicate cut axons. Scale bar, 50 μm.

In (A), (C), and (D), a black bar represents the median. N.S., not significant; **p < 0.01, ***p < 0.001, 2-tailed K-S test.

Expression of this hybrid construct resulted in GFP expression and also increased regeneration. In contrast, expression of GFP with a control 3′ UTR did not affect regeneration, although similar levels of GFP fluorescence were observed (Figures 3A, S2C, and S2D). Of note, the experiments shown in Figure 3A were performed in a completely wild-type background; neurons were visualized using GFP produced from these arrays rather than from the integrated GFP marker *oxIs12*. Thus, these data indicate that the regeneration-enhancing effect of the *xbp-1* 3′ fragment is not dependent on *oxIs12*. Most importantly, these experiments also indicate that the regeneration-promoting activity of the *xbp-1* 3′ fragment is contained within the 3′ UTR, suggesting that the *xbp-1* 3′ fragment acts as a ncRNA.

The endogenous *xbp-1* 3′ fragment is produced in the cytoplasm by cleavage of the *xbp-1*^{U} transcript on the ER membrane. On the other hand, the overexpressed *xbp-1* 3′ fragment is transcribed in the nucleus. Proper pre-mRNA processing and messenger ribonucleoprotein (mRNP) assembly is required for mRNA stability and efficient export into the cytoplasm (Maniatis and Reed, 2002). Consistent with this idea, we found that the *xbp-1* 3′ fragment only increases regeneration when it contains at least one intron, which is likely to promote nuclear export (Maniatis and Reed, 2002; Figures S2E and S2F). Deletion of the start codon (rather than frameshifting it) also abolished the overexpressed construct's ability to promote regeneration (Figure S2B), perhaps because of an effect on RNA stability or export. To construct a minimal functional sequence without any introns, start codons, or coding potential, we fused the *xbp-1* 3′ UTR with the retrovirus-derived constitutive transport element (CTE). The CTE RNA sequence hijacks the cellular mRNA nuclear export machinery and is exported independent of mRNA processing (Ernst et al., 1997; Grüter et al., 1998). We found that expression of this minimal construct (CTE-UTR) increased axon regeneration (Figure 3B), similar to expression of the entire *xbp-1* 3′ fragment (Figure 2C). Together, these data support the idea that the *xbp-1* 3′ fragment acts as a ncRNA to promote regeneration and that cytoplasmic localization is essential for its function.

The Function of the *xbp-1* ncRNA Depends on an RNA Stem

To determine which region of the *xbp-1* 3′ fragment is required for its function in regeneration, we tested a series of truncations of the 3′ fragment (Figure 3C) expressed under a GABA-specific promoter. The results were consistent with our findings that the coding sequence is dispensable because deletions in this region preserved function (Figure 3D, Δ1–189 and Δ190–378). In contrast, we found that a 189-nt region in the predicted 3′ UTR

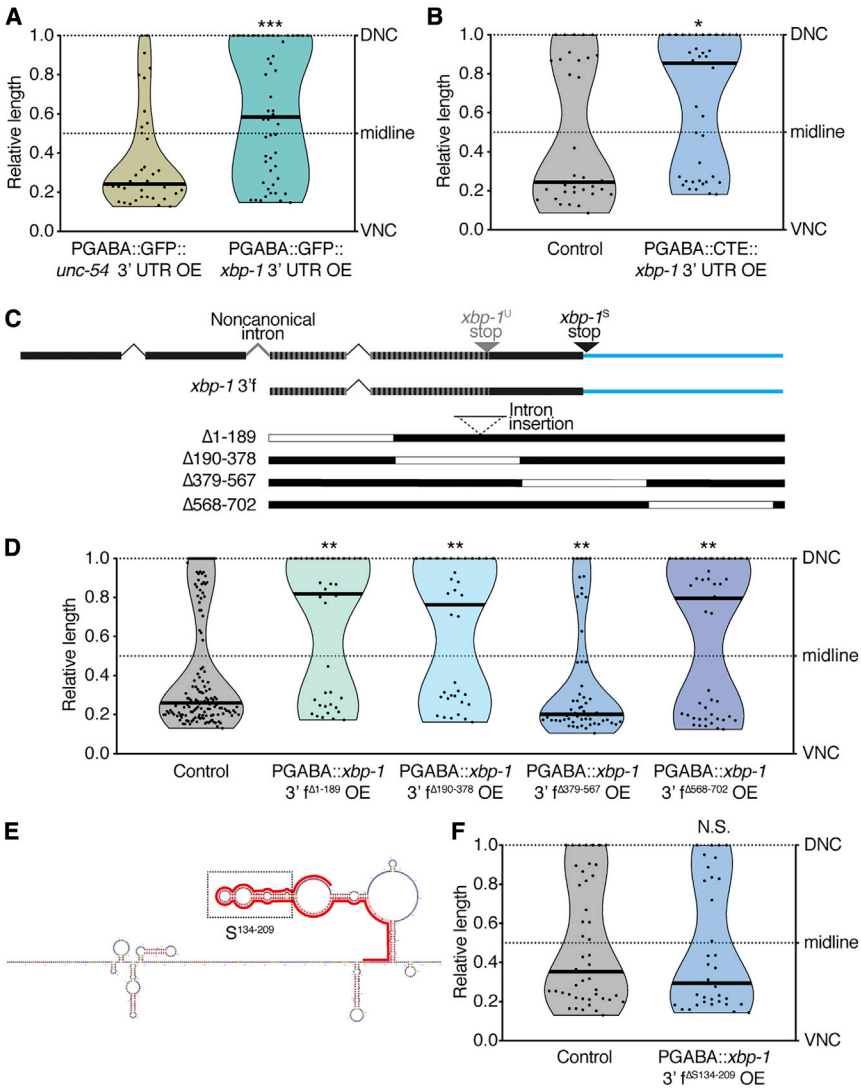

Figure 3. The *xbp-1* 3′ UTR Promotes Axon Regeneration as a ncRNA

(A) The *xbp-1* 3′ UTR increases regeneration even when fused to the GFP coding sequence. See Figure S2D for representative micrographs showing GFP expression. To visualize GFP fluorescence, these constructs were expressed in a wild-type N2 background as opposed to the *oxIs12* background (GABA-specific GFP marker) used in other axotomy experiments. Regeneration was scored 14 h (instead of 24 h) after axotomy. n = 42 and 50 from left to right. See also Figures S2C and S2D.

(B) When exported from the nucleus into the cytoplasm with the help of CTE, the *xbp-1* 3′ UTR increases regeneration without any coding sequence. n = 35 and 39 from left to right.

(C) Diagrams of *xbp-1* 3′ fragment deletion constructs.

(D) Axotomy results of animals expressing the constructs in (C). n = 148, 39, 36, 57, and 48 from left to right.

(E) Predicted secondary structure of the *xbp-1* 3′ fragment based on SHAPE-MaP results.

(F) The *xbp-1* 3′ fragment with the RNA stem $S^{134–209}$ deleted no longer promotes axon regeneration. n = 47 and 34 from left to right.

In (A), (B), (D), and (F), a black bar represents the median. *p < 0.05, **p < 0.01, ***p < 0.001, 2-tailed K-S test.

is required for the 3′ fragment to increase regeneration (Figure 3D, Δ379–567). *In silico* folding by Vienna RNAfold of this region indicated that it contains a high-probability RNA stem, which was confirmed by selective 2′-hydroxyl acylation analyzed by primer extension and mutational profiling (SHAPE-MaP) (Siegfried et al., 2014) performed on *in-vitro*-transcribed and folded RNAs (Figure 3E). We hypothesized that this stem (nucleotides 134–209 from the start of the *xbp-1* 3′ UTR, called $S^{134–209}$ hereafter) could be a functional element of the *xbp-1* 3′ fragment. In support of this, deleting $S^{134–209}$ was sufficient to abolish the function of the *xbp-1* 3′ fragment (compare Figures 3F and 2C).

To further explore the function of $S^{134–209}$, we began by observing that the *xbp-1* 3′ UTR (which contains $S^{134–209}$) does not function under every condition. The *xbp-1* 3′ UTR promotes regeneration when expressed as part of the *xbp-1* 3′ fragment (Figure 2C), when attached to the GFP coding sequence (GFP-UTR; Figure 3A), or when fused to CTE (CTE-UTR; Figure 3B). In contrast, we found that it does not have a significant effect on regeneration when it is part of the full-length *xbp-1* transcript. The *xbp-1(uncleavable)* allele has poor regeneration even though the 3′ UTR is present (Figure 1F), and overexpression of either wild-type or uncleavable full-length *xbp-1* with the 3′ UTR under a GABA-specific promoter does not increase regeneration (Figure 4A). These data suggest that the *xbp-1* 3′ UTR, and perhaps the key $S^{134–209}$ region, is in an inactive structural conformation when part of the full-length *xbp-1* transcript.

We used SHAPE-MaP to compare the RNA structures of the active RNAs (*xbp-1* 3′ fragment, CTE-UTR, and GFP-UTR) with the inactive RNA (full-length *xbp-1*). We focused on the $S^{134–209}$ sequence because our analysis demonstrated that it is necessary for function (Figure 3F). SHAPE-MaP identified a single nucleotide within $S^{134–209}$ whose reactivity differences correlated with the different function of the RNAs (Figures 4B and S3A). Specifically, C159 shows low SHAPE reactivity and is predicted to be paired in a stem structure in the three active RNAs (Figures 4C, left, and S3B). On the other hand, in the inactive full-length *xbp-1* RNA, C159 is highly accessible, indicating that the stem containing it does not form (Figures 4C, right, and S3B). These *in vitro* SHAPE data suggest that pairing at C159 may be critical *in vivo* for the function of the *xbp-1* ncRNA. To test the functional importance of C159 pairing, we mutated it to G (C159G; Figure 4C, box) in the CTE-UTR construct. This single mutation completely abolished the ability of the CTE-UTR

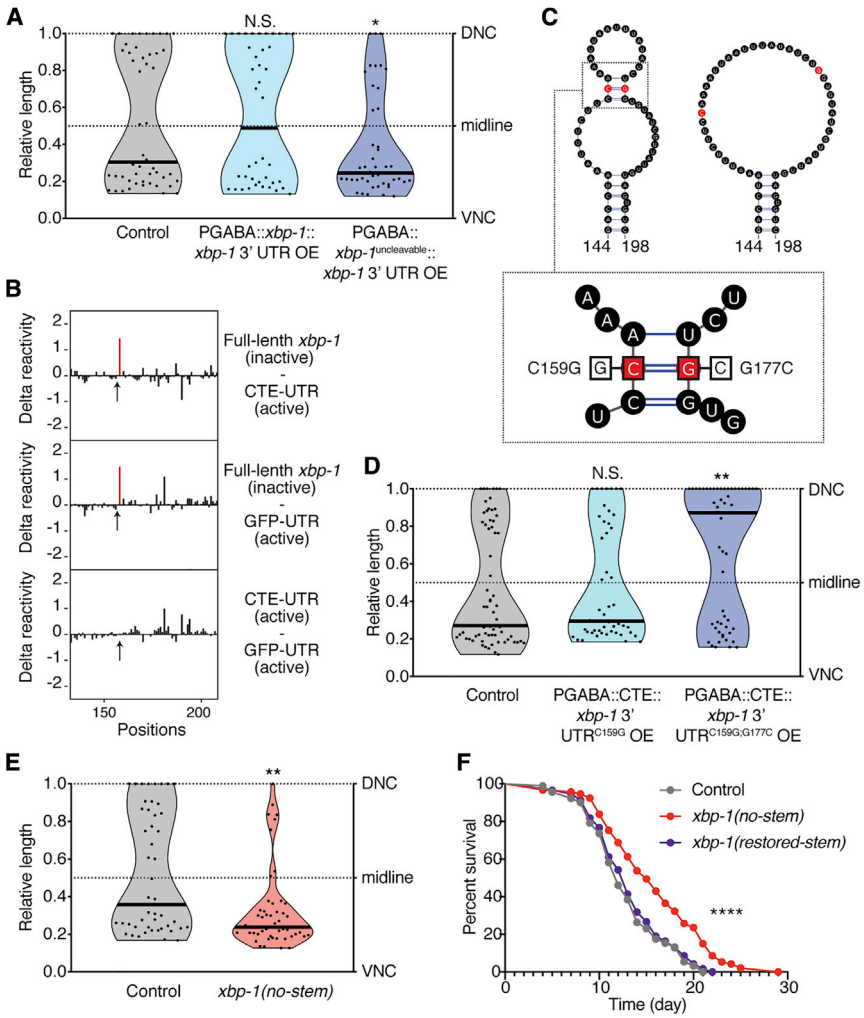

Figure 4. A Single Base Pair within S$^{134–209}$ Is Essential for *xbp-1* ncRNA Function

(A) Overexpression of the full-length *xbp-1* transcript does not increase regeneration. n = 50, 41, and 45 from left to right.

(B) Base-by-base comparisons of SHAPE reactivity differences across the length of S$^{134–209}$. Arrows point to C159.

(C) Predicted secondary structures of partial S$^{134–209}$ based on SHAPE-MaP results. Left: the active forms (*xbp-1* 3′ fragment, CTE-UTR, and GFP-UTR). Right: the inactive form (full-length *xbp-1*). Box inset: diagram of point mutations used in (D)–(F).

(D) Base-pairing at C159 is essential for the overexpressed CTE::*xbp-1* 3′ UTR to increase regeneration. n = 67, 48, and 55 from left to right.

(E) C159G mutation at the endogenous *xbp-1* locus decreases regeneration. n = 49 and 50 from left to right.

(F) The endogenous *xbp-1* ncRNA affects animal lifespan. n = 91, 93, and 116 from top to bottom. ****p < 0.0001, log rank Mantel-Cox test.

In (A), (D), and (E), a black bar represents the median. *p < 0.05, **p < 0.01, 2-tailed K-S test. See also Figure S3.

construct to promote regeneration (compare Figures 4D and 3B). Next we introduced a compensatory mutation (G177C; Figure 4C, box) that our structural analysis predicted would restore base-pairing and stem formation. This second mutation restored the regeneration-promoting activity of the CTE-UTR construct (Figure 4D). Together, these results confirm that the CTE-UTR construct acts as a ncRNA and demonstrate that pairing at C159 is required for function.

xbp-1 ncRNA Is Essential for *In Vivo* Axon Regeneration

The endogenous *xbp-1* transcript encodes the XBP-1 protein and has a well-established role in the XBP-UPR. Our experiments show that overexpressed fragments of this transcript can also act as ncRNAs. But does the endogenous *xbp-1* transcript give rise to a ncRNA in addition to its coding function? To determine the potential ncRNA function of the *xbp-1* 3′ fragment in its natural context, we used CRISPR to engineer the C159G-equivalent (Figure 4C, box) change into the endogenous *xbp-1* locus (*xbp-1(no-stem)*). In contrast to the *xbp-1(uncleavable)* and *xbp-1(deletion)* alleles, *xbp-1(no-stem)* animals have a normal XBP-1 protein-mediated UPR (Figure S3C). Thus, the *xbp-1(no-stem)* allele does not affect the coding output of the endogenous *xbp-1* transcript, as expected from a single-nucleotide change in the 3′ UTR. However, *xbp-1(no-stem)* animals have significantly impaired regeneration compared with control animals (Figure 4E). The loss of regeneration is nearly as strong as in the *xbp-1(uncleavable)* and *xbp-1(deletion)* alleles (Figures 1F and 2D), indicating that C159 is required for the function of the endogenous, non-coding *xbp-1* 3′ fragment *in vivo*. Next, we CRISPR-engineered the G177C-equivalent (Figure 4C, box) change into the *xbp-1(no-stem)* allele to restore the predicted base-pairing of endogenous *xbp-1* ncRNA (*xbp-1(restored-stem)*). In the RtcB mutant background, in which the ncRNA fragment accumulates and results in high regeneration, we observed a strikingly significant increase in regeneration in *xbp-1(restored-stem)* animals compared with *xbp-1(no-stem)* animals (Figure S3D). Restoring the stem did not have a significant effect in the RtcB wild-type background (Figure S3E), although some neurons were able to regenerate fully to the dorsal nerve cord, which was never observed in *xbp-1(no-stem)* animals (p = 0.058, 2-tailed Fisher's exact test). Together, these data indicate that the endogenous *xbp-1* 3′ fragment acts as a ncRNA and support the idea that the stem structure is a key functional element. In addition to the structure of the stem, sequence elements in the stem appear to play an auxiliary role in certain contexts.

The non-coding output of the endogenous *xbp-1* transcript affects more than just axon regeneration. We found that *xbp-1(no-stem)* animals have a significantly longer lifespan compared with control animals (Figure 4F). Similar to regeneration, this effect is

also dependent on base-pairing at the C159 site because the long lifespan was fully restored to normal in *xbp-1(restored-stem)* animals. Taken together, our data indicate that, in its natural context, *xbp-1* mediates a non-coding pathway that is separable from its coding-dependent function and that the endogenous *xbp-1* ncRNA affects axon regeneration and animal lifespan.

DISCUSSION

RNA Processing Intermediates with Unidentified Functions

The *xbp-1*^{U} transcript undergoes a well-conserved non-canonical splicing pathway, where an endonuclease and a ligase act sequentially to generate the protein-coding *xbp-1*^{S} transcript. Although previous studies of the output of the *xbp-1* pathway focused on the function of the *xbp-1*^{S} transcript, which encodes the critical UPR mediator XBP-1, our work reveals an unexpected role of a processing intermediate fragment of this pathway. We report that this intermediate RNA fragment functions as a ncRNA entirely independent of the XBP-UPR.

More broadly, our data support the concept that RNA processing events like RNA cleavage can produce functional intermediate fragments in addition to the final product. This phenomenon has been observed previously, with the most well-documented example being tRNA fragments (Hanada et al., 2013; Sobala and Hutvagner, 2011; Thompson and Parker, 2009). However, prior to this study, it was not known whether mRNA cleavage would also result in RNA fragments with non-coding functions. mRNA cleavage is a widespread cellular event. For example, during regulated IRE1-dependent decay (RIDD) of mRNA, numerous mRNAs are cleaved by the endonuclease IRE-1 (Hollien et al., 2009). Our study widens the potential landscape of ncRNAs produced by cleavage to include those produced from mature mRNAs.

Roles of *xbp-1* in Regulating the Neuronal Injury Response

The *xbp-1* locus has been shown to function in neuronal injury across species (Hu et al., 2012; Kosmaczewski et al., 2015; Ohtake et al., 2018; Oñate et al., 2016; Song et al., 2015; Ying et al., 2015). It has been linked to axon regeneration itself as well as to related cellular activities such as cell survival, myelin removal, and microphage infiltration (Hu et al., 2012; Oñate et al., 2016). Our work identifies a novel mechanism by which the *xbp-1* locus functions in neuronal injury: via a ncRNA generated by *xbp-1* mRNA cleavage. The cellular mechanisms that mediate the non-coding function of the *xbp-1* 3′ fragment remain to be determined. In general, ncRNAs can function via diverse mechanisms, including acting as enzymes, ligands, structural scaffolds, and molecular sponges (Fu, 2014; Ponting et al., 2009). For the *xbp-1* 3′ fragment, one or more of these mechanisms might impinge on the cellular pathways that mediate axon regeneration; for example, the well-characterized DLK-1 pathway (Hammarlund et al., 2009; Yan et al., 2009), which has a similar effect size on regeneration as the *xbp-1* ncRNA. In addition, the *xbp-1* 3′ fragment influences lifespan, perhaps via independent cellular pathways. Further experiments will be necessary to describe how the *xbp-1* ncRNA functions and to identify the cellular mechanisms it affects.

The Endogenous *xbp-1* Transcript Has Coding/Non-coding Dual Outputs

RNA molecules are generally divided into two worlds with little overlap: coding and non-coding. Our data identify *xbp-1* as the first ncRNA that is directly derived from cleavage of a mature mRNA. Thus, the endogenous *xbp-1* transcript has coding/non-coding dual outputs. The coding output mediates the XBP-UPR. The non-coding output is mediated by the *xbp-1* 3′ fragment. It affects axon regeneration and animal lifespan. Our work thus places the *xbp-1* RNA into the small group of RNAs that act as coding and ncRNAs, sometimes called coding and ncRNAs (cncRNAs) (Crerar et al., 2019; DeJesus-Hernandez et al., 2011; Ji et al., 2015; Kumari and Sampath, 2015; Mori et al., 2013; Sampath and Ephrussi, 2016). Such RNAs blur the line between the coding and ncRNA worlds and raise the question of how their dual roles are regulated.

In the case of *xbp-1*, the coding/non-coding dual outputs may be regulated by modulating the balance between cleavage and ligation. Although regulation of cleavage of *xbp-1* mRNA by IRE-1 has been characterized extensively, less is known about regulation of ligation by RtcB. However, multiple potential avenues for ligation regulation exist. First, although *in vitro* RtcB exhibits RNA ligase activity on its own, *in vivo* it is thought to act as the catalytic subunit of a complex that includes archease and DDX1 (Desai et al., 2014, 2015; Popow et al., 2014). RtcB has also been reported to complex *in vivo* with multiple other accessory proteins, like FAM98B and hCLE/C14orf166/RTRAF (Kanai et al., 2004; Pazo et al., 2019; Pérez-González et al., 2014). These interactions may affect ligase function and provide a mechanism for regulation. Second, RNA ligation by RtcB requires specific chemistry at the RNA ends to be joined; a number of factors, including the cyclic phosphodiesterase CNP, the RNA cyclase RtcA (Unlu et al., 2018), as well as cytoplasmic capping machinery, could potentially alter this chemistry. Such modifications could also affect the stability of the cleaved fragments because the 5′ fragment has been shown in yeast to be degraded by exonuclease when not ligated (Peschek and Walter, 2019). Third, RtcB can be transported by kinesin along microtubules in neurons (Kanai et al., 2004). We previously observed that RtcB translocates to severed axon tips after injury (Kosmaczewski et al., 2015). Thus, ligation could be modulated by subcellular localization. Injury and other cellular stresses might act via one or more of these regulatory mechanisms to shift the cleavage-ligation balance and regulate *xbp-1* ncRNA function.

Our study indicates that cleavage and ligation modulate the function of the *xbp-1* ncRNA because they have a secondary effect on RNA structure. We hypothesize that suppression of ncRNA function in the full-length *xbp-1* transcript is due to interaction with specific sequences within the 5′ fragment sequence. This interaction would inhibit ncRNA function in the uncleaved mRNA (*xbp-1*^{U}) and the ligated mRNA (*xbp-1*^{S}) but allow ncRNA function in the unligated 3′ fragment or when the *xbp-1* ncRNA is placed in the context of a different mRNA (encoding GFP). We find that cleavage—and, presumably, removal of inhibition—

causes a structural switch in the *xbp-1* 3′ fragment, activating its non-coding function. Specifically, cleavage favors formation of a stem-loop structure within the *xbp-1* 3′ UTR by base-pairing at the C159G site. This may, in turn, allow the ncRNA to interact with downstream effectors. Stem-loop structures are also predicted in the 3′ UTR of the *xbp-1* homologs in other organisms, but such structures are common in UTR regions, and their functional significance remains to be determined. Our data regarding *C. elegans* indicate that cleavage-induced structural switching is a novel mechanism to switch between the coding and non-coding outputs of a cncRNA depending on the status of the cell. In the case of *xbp-1*, cells can use this switch to fine-tune their response to injury and other stresses via different cellular responses.

STAR★METHODS

Detailed methods are provided in the online version of this paper and include the following:

- KEY RESOURCES TABLE
- RESOURCE AVAILABILITY
  - Lead Contact
  - Materials Availability
  - Data and Code Availability
- EXPERIMENTAL MODEL AND SUBJECT DETAILS
  - Caenorhabditis elegans
- METHOD DETAILS
  - Transgenic animal generation
  - CRISPR Mutations
  - Molecular Biology
  - xbp-1 RT-PCR assay
  - UPR Fluorescent Reporter Assay
  - Imaging of live animals
  - Laser Axotomy
  - Northern blots
  - RNA sequencing
  - SHAPE-MaP
  - Lifespan assay
- QUANTIFICATION AND STATISTICAL ANALYSIS
  - Analysis of axotomy data
  - Analysis of lifespan data
  - Splice junction analysis of RNA-seq data
  - Analysis of SHAPE-MaP data

SUPPLEMENTAL INFORMATION

Supplemental Information can be found online at https://doi.org/10.1016/j.neuron.2020.06.015.

ACKNOWLEDGMENTS

This research was supported by the Gruber Science Fellowship (to X.L. and C.A.D.), K99 award HD093873 from the NIH; the Eunice Kennedy Shriver National Institute of Child Health and Human Development (NICHD) (to J.-D.B.), NIH grant R35 GM122580 (to A.J.G.), and NIH grants R01 NS098817 and R01 NS094219 (to M.H.). We thank WormBase and the Caenorhabditis Genetics Center (CGC), which is funded by the NIH Office of Research Infrastructure Programs (P40 OD010440). We thank the Steitz lab at Yale University, especially Dr. Joan A. Steitz and Dr. Johanna Withers, for sharing reagents, protocols, and space for our northern blots.

AUTHOR CONTRIBUTIONS

X.L., J.-D.B., S.G.K., C.A.D., and M.H. designed the experiments. X.L. performed the experiments and data analysis. S.G.K., B.I.M., and J.-D.B. performed the RNA-seq experiments. J.-D.B. performed the splice junction analysis with help from S.G.K. and X.L. J.-D.B. performed the SHAPE-MaP experiments and processed the SHAPE-MaP data. C.A.D. performed the lifespan assay. All authors discussed and interpreted the results. M.H. supervised the project with contribution from A.J.G. X.L., and M.H. prepared the manuscript with input from the other authors.

DECLARATION OF INTERESTS

The authors declare no competing interests.

Received: January 6, 2020
Revised: May 23, 2020
Accepted: June 15, 2020
Published: July 7, 2020

REFERENCES

Arribere, J.A., Bell, R.T., Fu, B.X.H., Artiles, K.L., Hartman, P.S., and Fire, A.Z. (2014). Efficient marker-free recovery of custom genetic modifications with CRISPR/Cas9 in Caenorhabditis elegans. Genetics *198*, 837–846.

Calfon, M., Zeng, H., Urano, F., Till, J.H., Hubbard, S.R., Harding, H.P., Clark, S.G., and Ron, D. (2002). IRE1 couples endoplasmic reticulum load to secretory capacity by processing the XBP-1 mRNA. Nature *415*, 92–96.

Crerar, H., Scott-Solomon, E., Bodkin-Clarke, C., Andreassi, C., Hazbon, M., Logie, E., Cano-Jaimez, M., Gaspari, M., Kuruvilla, R., and Riccio, A. (2019). Regulation of NGF Signaling by an Axonal Untranslated mRNA. Neuron *102*, 553–563.e8.

DeJesus-Hernandez, M., Mackenzie, I.R., Boeve, B.F., Boxer, A.L., Baker, M., Rutherford, N.J., Nicholson, A.M., Finch, N.A., Flynn, H., Adamson, J., et al. (2011). Expanded GGGGCC hexanucleotide repeat in noncoding region of C9ORF72 causes chromosome 9p-linked FTD and ALS. Neuron *72*, 245–256.

Desai, K.K., Cheng, C.L., Bingman, C.A., Phillips, G.N., Jr., and Raines, R.T. (2014). A tRNA splicing operon: Archease endows RtcB with dual GTP/ATP cofactor specificity and accelerates RNA ligation. Nucleic Acids Res. *42*, 3931–3942.

Desai, K.K., Beltrame, A.L., and Raines, R.T. (2015). Coevolution of RtcB and Archease created a multiple-turnover RNA ligase. RNA *21*, 1866–1872.

Dickinson, D.J., Ward, J.D., Reiner, D.J., and Goldstein, B. (2013). Engineering the Caenorhabditis elegans genome using Cas9-triggered homologous recombination. Nat. Methods *10*, 1028–1034.

Dobin, A., Davis, C.A., Schlesinger, F., Drenkow, J., Zaleski, C., Jha, S., Batut, P., Chaisson, M., and Gingeras, T.R. (2013). STAR: ultrafast universal RNA-seq aligner. Bioinformatics *29*, 15–21.

Edelstein, A.D., Tsuchida, M.A., Amodaj, N., Pinkard, H., Vale, R.D., and Stuurman, N. (2014). Advanced methods of microscope control using μManager software. J. Biol. Methods *1*, 10.

Englert, M., Sheppard, K., Aslanian, A., Yates, J.R., 3rd, and Söll, D. (2011). Archaeal 3′-phosphate RNA splicing ligase characterization identifies the missing component in tRNA maturation. Proc. Natl. Acad. Sci. USA *108*, 1290–1295.

Ernst, R.K., Bray, M., Rekosh, D., and Hammarskjöld, M.L. (1997). A structured retroviral RNA element that mediates nucleocytoplasmic export of intron-containing RNA. Mol. Cell. Biol. *17*, 135–144.

Farboud, B., and Meyer, B.J. (2015). Dramatic enhancement of genome editing by CRISPR/Cas9 through improved guide RNA design. Genetics *199*, 959–971.

Fu, X.-D. (2014). Non-coding RNA: a new frontier in regulatory biology. Natl. Sci. Rev. *1*, 190–204.

Gonzalez, T.N., Sidrauski, C., Dörfler, S., and Walter, P. (1999). Mechanism of non-spliceosomal mRNA splicing in the unfolded protein response pathway. EMBO J. *18*, 3119–3132.

Grüter, P., Tabernero, C., von Kobbe, C., Schmitt, C., Saavedra, C., Bachi, A., Wilm, M., Felber, B.K., and Izaurralde, E. (1998). TAP, the human homolog of Mex67p, mediates CTE-dependent RNA export from the nucleus. Mol. Cell *1*, 649–659.

Hammarlund, M., Jorgensen, E.M., and Bastiani, M.J. (2007). Axons break in animals lacking β-spectrin. J. Cell Biol. *176*, 269–275.

Hammarlund, M., Nix, P., Hauth, L., Jorgensen, E.M., and Bastiani, M. (2009). Axon regeneration requires a conserved MAP kinase pathway. Science *323*, 802–806.

Hanada, T., Weitzer, S., Mair, B., Bernreuther, C., Wainger, B.J., Ichida, J., Hanada, R., Orthofer, M., Cronin, S.J., Komnenovic, V., et al. (2013). CLP1 links tRNA metabolism to progressive motor-neuron loss. Nature *495*, 474–480.

Hetz, C., and Mollereau, B. (2014). Disturbance of endoplasmic reticulum proteostasis in neurodegenerative diseases. Nat. Rev. Neurosci. *15*, 233–249.

Hollien, J., and Weissman, J.S. (2006). Decay of endoplasmic reticulum-localized mRNAs during the unfolded protein response. Science *313*, 104–107.

Hollien, J., Lin, J.H., Li, H., Stevens, N., Walter, P., and Weissman, J.S. (2009). Regulated Ire1-dependent decay of messenger RNAs in mammalian cells. J. Cell Biol. *186*, 323–331.

Hu, Y., Park, K.K., Yang, L., Wei, X., Yang, Q., Cho, K.-S., Thielen, P., Lee, A.-H., Cartoni, R., Glimcher, L.H., et al. (2012). Differential effects of unfolded protein response pathways on axon injury-induced death of retinal ganglion cells. Neuron *73*, 445–452.

Ji, Z., Song, R., Regev, A., and Struhl, K. (2015). Many lncRNAs, 5′UTRs, and pseudogenes are translated and some are likely to express functional proteins. eLife *4*, e08890.

Jiang, D., Niwa, M., and Koong, A.C. (2015). Targeting the IRE1α-XBP1 branch of the unfolded protein response in human diseases. Semin. Cancer Biol. *33*, 48–56.

Jurkin, J., Henkel, T., Nielsen, A.F., Minnich, M., Popow, J., Kaufmann, T., Heindl, K., Hoffmann, T., Busslinger, M., and Martinez, J. (2014). The mammalian tRNA ligase complex mediates splicing of XBP1 mRNA and controls antibody secretion in plasma cells. EMBO J. *33*, 2922–2936.

Kanai, Y., Dohmae, N., and Hirokawa, N. (2004). Kinesin transports RNA: isolation and characterization of an RNA-transporting granule. Neuron *43*, 513–525.

Kawahara, T., Yanagi, H., Yura, T., and Mori, K. (1998). Unconventional splicing of HAC1/ERN4 mRNA required for the unfolded protein response. Sequence-specific and non-sequential cleavage of the splice sites. J. Biol. Chem. *273*, 1802–1807.

Kosmaczewski, S.G., Edwards, T.J., Han, S.M., Eckwahl, M.J., Meyer, B.I., Peach, S., Hesselberth, J.R., Wolin, S.L., and Hammarlund, M. (2014). The RtcB RNA ligase is an essential component of the metazoan unfolded protein response. EMBO Rep. *15*, 1278–1285.

Kosmaczewski, S.G., Han, S.M., Han, B., Irving Meyer, B., Baig, H.S., Athar, W., Lin-Moore, A.T., Koelle, M.R., and Hammarlund, M. (2015). RNA ligation in neurons by RtcB inhibits axon regeneration. Proc. Natl. Acad. Sci. USA *112*, 8451–8456.

Kumari, P., and Sampath, K. (2015). cncRNAs: Bi-functional RNAs with protein coding and non-coding functions. Semin. Cell Dev. Biol. *47-48*, 40–51.

Langmead, B., and Salzberg, S.L. (2012). Fast gapped-read alignment with Bowtie 2. Nat. Methods *9*, 357–359.

Lu, Y., Liang, F.-X., and Wang, X. (2014). A synthetic biology approach identifies the mammalian UPR RNA ligase RtcB. Mol. Cell *55*, 758–770.

Maniatis, T., and Reed, R. (2002). An extensive network of coupling among gene expression machines. Nature *416*, 499–506.

Mori, K., Weng, S.-M., Arzberger, T., May, S., Rentzsch, K., Kremmer, E., Schmid, B., Kretzschmar, H.A., Cruts, M., Van Broeckhoven, C., et al. (2013). The C9orf72 GGGGCC repeat is translated into aggregating dipeptide-repeat proteins in FTLD/ALS. Science *339*, 1335–1338.

Nix, P., Hammarlund, M., Hauth, L., Lachnit, M., Jorgensen, E.M., and Bastiani, M. (2014). Axon regeneration genes identified by RNAi screening in C. elegans. J. Neurosci. *34*, 629–645.

Ohtake, Y., Matsuhisa, K., Kaneko, M., Kanemoto, S., Asada, R., Imaizumi, K., and Saito, A. (2018). Axonal Activation of the Unfolded Protein Response Promotes Axonal Regeneration Following Peripheral Nerve Injury. Neuroscience *375*, 34–48.

Oñate, M., Catenaccio, A., Martínez, G., Armentano, D., Parsons, G., Kerr, B., Hetz, C., and Court, F.A. (2016). Activation of the unfolded protein response promotes axonal regeneration after peripheral nerve injury. Sci. Rep. *6*, 21709.

Paix, A., Wang, Y., Smith, H.E., Lee, C.-Y.S., Calidas, D., Lu, T., Smith, J., Schmidt, H., Krause, M.W., and Seydoux, G. (2014). Scalable and versatile genome editing using linear DNAs with microhomology to Cas9 Sites in Caenorhabditis elegans. Genetics *198*, 1347–1356.

Pazo, A., Pérez-González, A., Oliveros, J.C., Huarte, M., Chavez, J.P., and Nieto, A. (2019). hCLE/RTRAF-HSPC117-DDX1-FAM98B: A New Cap-Binding Complex That Activates mRNA Translation. Front. Physiol. *10*, 92.

Pérez-González, A., Pazo, A., Navajas, R., Ciordia, S., Rodriguez-Frandsen, A., and Nieto, A. (2014). hCLE/C14orf166 associates with DDX1-HSPC117-FAM98B in a novel transcription-dependent shuttling RNA-transporting complex. PLoS ONE *9*, e90957.

Peschek, J., and Walter, P. (2019). tRNA ligase structure reveals kinetic competition between non-conventional mRNA splicing and mRNA decay. eLife *8*, e44199.

Ponting, C.P., Oliver, P.L., and Reik, W. (2009). Evolution and functions of long noncoding RNAs. Cell *136*, 629–641.

Popow, J., Englert, M., Weitzer, S., Schleiffer, A., Mierzwa, B., Mechtler, K., Trowitzsch, S., Will, C.L., Luhrmann, R., Soll, D., et al. (2011). HSPC117 Is the Essential Subunit of a Human tRNA Splicing Ligase Complex. Science *331*, 760–764.

Popow, J., Jurkin, J., Schleiffer, A., and Martinez, J. (2014). Analysis of orthologous groups reveals archease and DDX1 as tRNA splicing factors. Nature *511*, 104–107.

Sampath, K., and Ephrussi, A. (2016). CncRNAs: RNAs with both coding and non-coding roles in development. Development *143*, 1234–1241.

Schneider, C.A., Rasband, W.S., and Eliceiri, K.W. (2012). NIH Image to ImageJ: 25 years of image analysis. Nat. Methods *9*, 671–675.

Sidrauski, C., and Walter, P. (1997). The transmembrane kinase Ire1p is a site-specific endonuclease that initiates mRNA splicing in the unfolded protein response. Cell *90*, 1031–1039.

Sidrauski, C., Cox, J.S., and Walter, P. (1996). tRNA ligase is required for regulated mRNA splicing in the unfolded protein response. Cell *87*, 405–413.

Siegfried, N.A., Busan, S., Rice, G.M., Nelson, J.A.E., and Weeks, K.M. (2014). RNA motif discovery by SHAPE and mutational profiling (SHAPE-MaP). Nat. Methods *11*, 959–965.

Smola, M.J., Rice, G.M., Busan, S., Siegfried, N.A., and Weeks, K.M. (2015). Selective 2′-hydroxyl acylation analyzed by primer extension and mutational profiling (SHAPE-MaP) for direct, versatile and accurate RNA structure analysis. Nat. Protoc. *10*, 1643–1669.

Sobala, A., and Hutvagner, G. (2011). Transfer RNA-derived fragments: origins, processing, and functions. Wiley Interdiscip. Rev. RNA *2*, 853–862.

Song, Y., Sretavan, D., Salegio, E.A., Berg, J., Huang, X., Cheng, T., Xiong, X., Meltzer, S., Han, C., Nguyen, T.-T., et al. (2015). Regulation of axon regeneration by the RNA repair and splicing pathway. Nat. Neurosci. *18*, 817–825.

Tanaka, N., and Shuman, S. (2011). RtcB is the RNA ligase component of an *Escherichia coli* RNA repair operon. J. Biol. Chem. *286*, 7727–7731.

Thompson, D.M., and Parker, R. (2009). Stressing out over tRNA cleavage. Cell *138*, 215–219.

Unlu, I., Lu, Y., and Wang, X. (2018). The cyclic phosphodiesterase CNP and RNA cyclase RtcA fine-tune noncanonical *XBP1* splicing during ER stress. J. Biol. Chem. *293*, 19365–19376.

Walter, P., and Ron, D. (2011). The unfolded protein response: from stress pathway to homeostatic regulation. Science *334*, 1081–1086.

Yan, D., Wu, Z., Chisholm, A.D., and Jin, Y. (2009). The DLK-1 kinase promotes mRNA stability and local translation in C. elegans synapses and axon regeneration. Cell *138*, 1005–1018.

Ying, Z., Zhai, R., McLean, N.A., Johnston, J.M., Misra, V., and Verge, V.M.K. (2015). The Unfolded Protein Response and Cholesterol Biosynthesis Link Luman/CREB3 to Regenerative Axon Growth in Sensory Neurons. J. Neurosci. *35*, 14557–14570.

Yoshida, H., Matsui, T., Yamamoto, A., Okada, T., and Mori, K. (2001). XBP1 mRNA is induced by ATF6 and spliced by IRE1 in response to ER stress to produce a highly active transcription factor. Cell *107*, 881–891.

STAR★METHODS

KEY RESOURCES TABLE

REAGENT or RESOURCE	SOURCE	IDENTIFIER
Chemicals, Peptides, and Recombinant Proteins		
Tunicamycin	Sigma-Aldrich	Cat # 654380
Levimisole	Santa Cruz	Cat # sc-205730
TRIzol Reagent	Invitrogen	Cat # 15596026
0.05 μm microbeads for axotomy	Polysciences	Cat # 08691
Critical Commercial Assays		
AffinityScript Multiple Temperature cDNA Synthesis Kit	Agilent	Cat # #200436
SuperScript III Reverse Transcriptase	Invitrogen	Cat # 18080093
AmpliScribe T7-Flash transcription kit	Epicenter	Cat # ASF3257
SuperScript II Reverse Transcriptase	Invitrogen	Cat # 18064014
Deposited Data		
RNA-seq comparing between RtcB mutant and control animals with and without neuronal injury	This manuscript	Table S1
Experimental Models: Organisms/Strains		
C.elegans: N2 wild-type	Caenorhabditis Genetics Center (CGC)	N2 (ancestral)
C.elegans: oxIs12[P*unc-47*::GFP, *lin-15+*] X (Note: GABA-specific GFP. The gray "Control" used in all axotomy plots)	Caenorhabditis Genetics Center (CGC)	WormBase ID: WBTransgene00001635
C.elegans: rtcb-1(*gk451*) I / hT2[*bli-4*(*e937*), *let-?*(*q782*), *qIs48*] I;III; *wpIs63*; *oxIs12* [P*unc-47*::GFP, *lin-15+*] X (Note: *rtcb-1* null)	Kosmaczewski et al., 2015	XE1728
C.elegans: zcIs4[P*hsp-4*::GFP] V (Note: UPR reporter)	Caenorhabditis Genetics Center (CGC)	SJ4005
C.elegans: xbp-1(*wp45*) III (Note: *xbp-1(uncleavable)*)	This manuscript	XE2037
C.elegans: xbp-1(*wp45*) III; *oxIs12*[P*unc-47*::GFP, *lin-15+*] X	This manuscript	XE2038
C.elegans: xbp-1(*wp45*) III; *zcIs4*[P*hsp-4*::GFP] V	This manuscript	XE2234
C.elegans: xbp-1(*wp46*) III (Note: *xbp-1(deletion)*)	This manuscript	XE2048
C.elegans: xbp-1(*wp46*) III; *oxIs12*[P*unc-47*::GFP, *lin-15+*] X	This manuscript	XE2049
C.elegans: xbp-1(*wp46*) III; *zcIs4*[P*hsp-4*::GFP] V	This manuscript	XE2235
C.elegans: rtcb-1(*gk451*) I; *xbp-1*(*zc12*) III / hT2[*bli-4*(*e937*), *let-?*(*q782*), *qIs48*] I;III; *wpIs63*; *oxIs12*[P*unc-47*::GFP, *lin-15+*] X (Note: *rtcb-1; xbp-1* double mutant)	This manuscript	XE1928
C.elegans: rtcb-1(*gk451*) I; *xbp-1*(*zc12*) III / hT2[*bli-4*(*e937*), *let-?*(*q782*), *qIs48*] I;III; *wpIs63*; *oxIs12*[P*unc-47*::GFP, *lin-15+*] X; *wpEx355*[Punc-*25*::*xbp-1*::*unc-54* 3′ UTR + P*myo-2*::mCherry]	This manuscript	XE2236

(*Continued on next page*)

Continued

REAGENT or RESOURCE	SOURCE	IDENTIFIER
C.elegans: rtcb-1(*gk451*) I; *xbp-1*(*zc12*) III / hT2[*bli-4*(*e937*), *let-?*(*q782*), *qIs48*] I;III; *wpIs63*; *oxIs12*[P*unc-47*::GFP, *lin-15*+] X; *wpEx356*[Punc-*25*::*xbp-1*::*xbp-1* 3′ UTR + P*myo-2*::mCherry]	This manuscript	XE2237
C.elegans: rtcb-1(*gk451*) I; *xbp-1*(*zc12*) III / hT2[*bli-4*(*e937*), *let-?*(*q782*), *qIs48*] I;III; *wpIs63*; *oxIs12*[P*unc-47*::GFP, *lin-15*+] X; *wpEx290*[P*xbp-1*::*xbp-1*::*xbp-1* 3′ UTR + P*myo-2*::mCherry]	This manuscript	XE1948
C.elegans: wpEx342[P*unc-25*::*xbp-1* 3′ fragment + P*myo-2*::mCherry]; *oxIs12* [P*unc-47*::GFP, *lin-15*+] X	This manuscript	XE2181
C.elegans: xbp-1(*wp46*) III; *wpEx342*[P*unc-25*::*xbp-1* 3′ fragment + P*myo-2*::mCherry]; *oxIs12*[P*unc-47*::GFP, *lin-15*+] X	This manuscript	XE2238
C.elegans: wpEx323[P*unc-25*::*xbp-1* 3′ fragment$^{\Delta AUG}$ + P*myo-2*::mCherry]; *oxIs12* [P*unc-47*::GFP, *lin-15*+] X	This manuscript	XE2063
C.elegans: wpEx322[P*unc-25*::*xbp-1* 3′ fragment$^{fs\text{-}AUG}$ + P*myo-2*::mCherry]; *oxIs12* [P*unc-47*::GFP, *lin-15*+] X	This manuscript	XE2062
C.elegans: wpEx329[P*unc-25*::GFP::*xbp-1* 3′UTR]	This manuscript	XE2094
C.elegans: wpEx357[P*unc-25*::GFP::*xbp-1* 3′UTR + P*myo-2*::mCherry]; *oxIs12*[P*unc-47*::GFP, *lin-15*+] X	This manuscript	XE2239
C.elegans: wpEx358[P*unc-25*::GFP::*unc-54* 3′UTR]	This manuscript	XE2240
C.elegans: wpEx359[P*unc-25*::GFP::*unc-54* 3′UTR + P*myo-2*::mCherry]; *oxIs12* [P*unc-47*::GFP, *lin-15*+] X	This manuscript	XE2241
C.elegans: wpEx341[P*unc-25*::CTE::*xbp-1* 3′ UTR + P*myo-2*::mCherry]; *oxIs12*[P*unc-47*::GFP, *lin-15*+] X	This manuscript	XE2180
C.elegans: wpEx327[P*unc-25*::*xbp-1* 3′ fragment$^{\Delta 1\text{-}189}$ + P*myo-2*::mCherry]; *oxIs12* [P*unc-47*::GFP, *lin-15*+] X	This manuscript	XE2092
C.elegans: wpEx325[P*unc-25*::*xbp-1* 3′ fragment$^{\Delta 190\text{-}378}$ + P*myo-2*::mCherry]; *oxIs12*[P*unc-47*::GFP, *lin-15*+] X	This manuscript	XE2067
C.elegans: wpEx353[P*unc-25*::*xbp-1* 3′ fragment$^{\Delta 379\text{-}567}$ + P*myo-2*::mCherry]; *oxIs12*[P*unc-47*::GFP, *lin-15*+] X	This manuscript	XE2231
C.elegans: wpEx354[P*unc-25*::*xbp-1* 3′ fragment$^{\Delta 568\text{-}702}$ + P*myo-2*::mCherry]; *oxIs12*[P*unc-47*::GFP, *lin-15*+] X	This manuscript	XE2232
C.elegans: wpEx326[P*unc-25*::*xbp-1* 3′ fragment$^{\Delta S134\text{-}209}$ + P*myo-2*::mCherry]; *oxIs12*[P*unc-47*::GFP, *lin-15*+] X	This manuscript	XE2072
C.elegans: wpEx309[P*unc-25*::*xbp-1*::*xbp-1* 3′ UTR + P*myo-2*::mCherry]; *oxIs12*[P*unc-47*::GFP, *lin-15*+] X	This manuscript	XE2034

(*Continued on next page*)

Continued

REAGENT or RESOURCE	SOURCE	IDENTIFIER
C.elegans: wpEx309[P*unc-25*::*xbp-1*^{uncleavable}::*xbp-1* 3′ UTR + P*myo-2*::mCherry]; *oxIs12*[P*unc-47*::GFP, *lin-15*+] X	This manuscript	XE2036
C.elegans: wpEx337[P*unc-25*::CTE::*xbp-1* 3′ UTR^{C159G} + P*myo-2*::mCherry]; *oxIs12* [P*unc-47*::GFP, *lin-15*+] X	This manuscript	XE2174
C.elegans: wpEx338[P*unc-25*::CTE::*xbp-1* 3′ UTR$^{C159G;\ G177C}$ + P*myo-2*::mCherry]; *oxIs12*[P*unc-47*::GFP, *lin-15*+] X	This manuscript	XE2175
C.elegans: xbp-1(*wp79*) III; *oxIs12*[P*unc-47*::GFP, *lin-15*+] X (Note: *xbp-1(no-stem)*)	This manuscript	XE2223
C.elegans: xbp-1(*wp79*) III; *zcIs4*[P*hsp-4*::GFP] V	This manuscript	XE2229
Oligonucleotides		
Forward primer for *xbp-1*^{U} and *xbp-1*^{S} in RT-PCR assay: GAGACAAAAAGAAG-GAAAGATCAGC	IDT	N/A
Reverse primer for *xbp-1*^{U} and *xbp-1*^{S} in RT-PCR assay: CTCCGCTTGGGCT-CTTGAGATG	IDT	N/A
Forward primer for *ama-1*^{S} control in RT-PCR assay: TGTCAGGATCGAAGGGATCGAAG	IDT	N/A
Reverse primer for *ama-1*^{S} control in RT-PCR assay: CGGTGAGGTCCAT-TCTGAAATC	IDT	N/A
Northern probes: see Table S3	This manuscript	N/A
Reverse transcription random primer used in RNA-seq library preparation: AGACGTGTGCTCTTCCGATCTNNNNNN	IDT	N/A
ssDNA adaptor used in RNA-seq library preparation: /5Phos/ NNNNNGATCGTCGGACTGTA GAACTCTGAAC/3InvdT/	IDT	N/A
In vitro transcribed RNA for SHAPE-MaP: See Table S4	This manuscript	N/A
Recombinant DNA		
pDD162	Dickinson et al., 2013	Addgene #47549
Software and Algorithms		
ImageJ	Schneider et al., 2012	https://imagej.nih.gov/ij/
Micro-Manager	Edelstein et al., 2014	https://micro-manager.org/
GraphPad Prism	GraphPad	https://www.graphpad.com/
CASAVA-1.8.2.	Illumina	http://bioweb.pasteur.fr/packages/pack@casava@1.8.2
Bowtie2 v2.2.4	Langmead and Salzberg, 2012	http://bowtie-bio.sourceforge.net/bowtie2/index.shtml
STAR version 2.4.2a	Dobin et al., 2013	https://github.com/alexdobin/STAR
Meta-chart	N/A	https://www.meta-chart.com/
ShapeMapper/SuperFold	Siegfried et al., 2014; Smola et al., 2015	http://chem.unc.edu/rna/software.html

RESOURCE AVAILABILITY

Lead Contact

Further information and requests for resources and reagents should be directed to and will be fulfilled by the Lead Contact, Marc Hammarlund (marc.hammarlund@yale.edu).

Materials Availability

Plasmids and worm lines generated in this study are available upon request.

Data and Code Availability

The published article includes all datasets generated or analyzed during this study.

EXPERIMENTAL MODEL AND SUBJECT DETAILS

Caenorhabditis elegans

C. elegans were maintained on nematode growth media (NGM) plates seeded with *Escherichia coli* OP50 at 20°C. Hermaphrodites were used for all experiments, and males were only used for crossing. The developmental stage of the animals used in each assay is reported in the Method Details section below.

METHOD DETAILS

Transgenic animal generation

For transgenic animals with extrachromosomal arrays, 20 ng/μL of relevant constructs were mixed with 2.5 ng/μL of P*myo-2*::mCherry (injection marker) and DNA ladder (Promega, G5711, to adjust the total concentration of the injection mix to ~150 ng/μL), and microinjected into the gonads of young adults. Transgenic animals were first selected based on the expression of P*myo-2*::mCherry, and then confirmed by PCR genotyping of the relevant constructs.

CRISPR Mutations

The four xbp-1 alleles (wp45, wp46, wp79, wp80) were generated by CRISPR as previously described (Arribere et al., 2014; Farboud and Meyer, 2015; Paix et al., 2014). Briefly, sgRNAs were ordered from IDT and cloned into our sgRNA plasmid backbone by simple PCR. Repair templates were either directly ordered from IDT (ssODN), or PCR amplified from genomic sequence (dsDNA). An injection mix of 50 ng/μL of pDD162 (P*eft-3*::Cas9), 40 ng/μL of relevant sgRNA(s), 30 ng/μL per 125 nt ssODN or per 50 nt dsDNA of repair template if using, 30 ng/μL of *dpy-10* sgRNA, and 26 ng/μL of ssODN AF-ZF-827 (*dpy-10* repair template), was injected into the gonads of young adults. F1 progenies of the injected parents were examined for *dpy-10* phenotype, and dumpy/roller worms were subject to sequencing. F2 progenies homozygous for the mutation were again confirmed by sequencing and were outcrossed > 3X prior to any experiments.

Molecular Biology

Gateway recombination (Invitrogen) was used to generate Punc-25::xbp-1::unc-54 3′ UTR, Punc-25::xbp-1::xbp-1 3′ UTR, Pxbp-1::xbp-1::xbp-1 3′ UTR, Punc-25::gfp::xbp-1 3′ UTR, and Punc-25::gfp::unc-54 3′ UTR. Gibson cloning was used to generate P*unc-25*::CTE::*xbp-1* 3′UTR and P*unc-25*::*xbp-1* 3′ fragment. The CTE sequence was synthesized by IDT. Other entry pieces were amplified using Phusion polymerase (NEB, M0530) from worm lysate or previous plasmids (Kosmaczewski et al., 2015). Gibson assembly was also used to generate the various deletion constructs on the basis of the P*unc-25*::*xbp-1* 3′ fragment construct. Site-directed mutagenesis was used to introduce the C159G and G177C point mutations to the P*unc-25*::CTE::*xbp-1* 3′UTR construct. All construct and primer sequences are available upon request.

xbp-1 RT-PCR assay

Worms of N2 wild-type, *xbp-1*(*wp45*) or *xbp-1*(*wp46*) were harvested from fully-populated NGM plates just before starving. Next, they were washed multiple times in M9 buffer, nutated in M9 with or without 5 μg/mL tunicamycin for 3 h, spun down, resuspended in TRIzol reagent (Invitrogen), frozen at −80°C overnight, and then subjected to freeze/thaw in liquid nitrogen/37°C incubator 3 times. RNA was isolated from the aqueous phase following manufacturer's instructions. First-strand cDNA was synthesized with AffinityScript Multiple Temperature cDNA Synthesis Kit (Agilent, #200436). PCR was carried out using Phusion polymerase (NEB, M0530) with intron-spanning primers listed in Key Resources Table. Products were digested with MseI (NEB, R0525) and then resolved on a 2% agarose gel.

UPR Fluorescent Reporter Assay

UPR assay was performed as described previously (Kosmaczewski et al., 2015). Briefly, animals at the L4 stage were placed on NGM plates with or without 5 μg/mL tunicamycin for 10-24 h as indicated. P*hsp-4*::GFP expression was then visualized by imaging.

Imaging of live animals

Animals were mounted on 3% (wt/vol) agarose pads and immobilized using 0.1% Levimisole (Santa Cruz, sc-205730). Images were taken with Olympus BX61 and processed with Micro-Manager.

Laser Axotomy

Laser axotomy was performed as described previously (Kosmaczewski et al., 2015). Briefly, worms at L4 stage were mounted on a 3% (wt/vol in M9 buffer) agarose pad, immobilized by 0.05 μm microbeads (Polysciences, #08691) with 0.02% SDS, and visualized with a Nikon Eclipse 80i Microscope. 3-4 of the 7 most posterior ventral and dorsal D-type (VD/DD) GABA motor neurons were severed using a Photonic Instruments Micropoint Laser at 10 pulses and 20 Hz. Worms were recovered to seeded NGM plates and scored for axon regeneration 24 h (unless otherwise stated) after axotomy.

Northern blots

~2,000 L4 N2 wild-type or *rtcb-1*(*gk451*) worms were picked to NGM plates with or without 50 μg/mL tunicamycin (*rtcb-1* homozygotes were isolated from balanced heterozygotes), incubated at 20°C for 3 h, and harvested from the plates with M9 buffer. RNA was isolated as in the *xbp-1* RT-PCR assay. 10 μg of total RNA was separated in 1.2% agarose-37% formaldehyde gels and transferred to Zeta-Probe membranes (Bio-Rad, 1620165) by capillary transfer in 20X SSC buffer for 22h. The blots were first hybridized and visualized with the following [^{32}P]-labeled oligonucleotide probes against the *xbp-1* sequence 3′ to the IRE-1 cleavage sites (*xbp-1* probes), and then stripped, and hybridized and visualized with *act-1* probes as control. The hybridized signals were visualized with the Storm 860 Molecular Imager (GMI). The sequences of the probes are listed in Table S3.

RNA sequencing

RNA-seq experiments were performed to identify RtcB-dependent changes in mRNA splicing. Samples were prepared in triplicate from the following four groups: control, *rtcb-1(gk451)*, *unc-70(s1502)*, and *rtcb-1(gk451)*; *unc-70(s1502)*. For each replicate, ~2,000 L4 worms were gathered. Total RNA was extracted using TRIzol as described above. Poly-A+ RNAs were isolated using oligo d(T)$_{25}$ magnetic beads (New England BioLabs) following the manufacturer's protocol and eluted in 11 μL of water. Reverse transcription was performed in 20 μL at 25°C for 10 min, 42°C for 30 min, 50°C for 10 min, 55°C for 20 min, and 60°C for 20 min, using Superscript III (Invitrogen) and reverse transcription random primer. The reaction was then heat inactivated at 75°C for 15 min and RNase H treated at 37°C for 15 min. cDNA samples were purified using 36 μL of AMPure XP beads (Beckman Coulter Life Sciences) following the manufacturer's protocol and eluted in 10 μL of water. Purified cDNA samples were ligated to a ssDNA adaptor at their 3′ end using CircLigase ssDNA Ligase (Epicenter) following the manufacturer's protocol with the addition of 1M betaine and 10% PEG 6000. Ligation reactions were incubated at 60°C for 2h, at 68°C for 1h and heat inactivated at 80°C for 10 min. 10 μL of water was added to each reaction and ligated products were purified using 36 μL of AMPure XP beads (Beckman Coulter Life Sciences) and dissolved in 16 μL of water. Purified ligated cDNA samples were then PCR amplified using Illumina sequencing adapters, keeping the number of cycles to the minimum needed for the detection of amplified products (8-12 cycles), and gel purified on 2% agarose gel to remove adaptor-adaptor dimers. Purified libraries were sequenced on Illumina HiSeq 2000/2500 machines producing single-end 76 nucleotide reads.

SHAPE-MaP

Four RNA species (*xbp-1* 3′ fragment, *gfp*::*xbp-1* 3′ UTR (GFP-UTR), CTE::*xbp-1* 3′ UTR (CTE-UTR), and *xbp-1*::*xbp-1* 3′ UTR (full-length *xbp-1*)) were transcribed *in vitro* from PCR products using the AmpliScribe T7-Flash transcription kit (Epicenter), and purified using RNeasy columns (QIAGEN). The primers used and the sequences of the RNAs generated are listed in Table S4. For each transcript, 1 μg of RNA in 14 μL final volume was heated to 95°C for 2 min, placed on ice for 2 min, folded at 22°C for 20 min with the addition of 4 μL of 5X folding buffer (500 mM tris HCl pH 7.5, 500 mM KCl and 50 mM MgCl2), probed at 22°C for 5 min with the addition of 2 μL NAI (2 M, Sigma-Aldrich) or DMSO, and quenched by the addition of 90 μL of stop solution (3 M β-mercaptoethanol, 508 mM sodium acetate and 15 μg glycoblue). Following a 5 min incubation at room temperature, samples were ethanol precipitated, washed with 70% ethanol, resuspended in water, and subjected to MaP reverse transcription (requiring Superscript II and the addition of Mn^{2+} to the RT buffer (Smola et al., 2015)) using random nonamer primers. Double-stranded cDNA was synthesized in Second Strand Synthesis Reaction Buffer (NEB) with Second Strand Synthesis Enzyme mix (NEB), purified using PureLink PCR micro spin column (Thermo Fisher Scientific), eluted in water, and sent to the Yale Center for Genome Analysis to be fragmented using the Nextera DNA Flex Library Prep Kit (Illumina) and sequenced on an Illumina NovaSeq sequencer producing paired-end 150 nucleotide reads.

Lifespan assay

For each genotype, ~100 L4 animals were picked to NGM plates seeded with OP50 bacteria. The animals were kept at 20°C and fed with OP50 during the assay. During the first 5 days, animals were transferred to a fresh seeded plate every other day to separate them from their off springs. Viability was scored every other day. Death was scored by failure to respond to touching.

QUANTIFICATION AND STATISTICAL ANALYSIS

Analysis of axotomy data

For all axotomy experiments, the relative lengths (Figure 1D) of all successfully cut axons (indicated by the presence of a severed distal stump) were measured with ImageJ and plotted with GraphPad Prism. All scoring processes were carried out blindly. No data were excluded. Measurements were taken from distinct samples for each plot shown. *n* represents the number of axons cut in each group (i.e., number of dots plotted in each violin), and the value of *n* can be found in figure legends. The black bar in each figure shows the median; median was used instead of mean because the distribution of relative length of cut axons is often not normal. Two-tailed *P value*s were calculated using the Kolmogorov-Smirnov test (2-tailed K-S test). The K-S test calculates empirical *P value* comparing the continuous probability distribution of a sample with a reference probability distribution, and does so by quantifying the distance between the two distribution functions. The K-S test does not assume or require normal distribution of the data. This is appropriate in our case because in many cases our data are not normally distributed. *P value*s are reported as asterisks in figures: *p < 0.05, **p < 0.01, ***p < 0.001, ****p < 0.0001.

Analysis of lifespan data

When conducting the lifespan assay, worms were counted dead only when the corpse could be found. Disappeared worms (which might have crawled out of plate or into cracks) were excluded. *n* represents the number of worms tested in each group, and the value of *n* can be found in figure legends. Survival curves were plotted with GraphPad Prism. Significance was calculated using the log rank Mantel-Cox test and is reported as asterisks in figures.

Splice junction analysis of RNA-seq data

Following the library preparation protocol, raw reads contained the following features: NNNNN-insert-adaptor, where the 5N sequence composes the Unique Molecular Identifier (UMI), and adaptor is the 3′-Illumina adaptor that can occasionally be present within the read (mainly in adaptor-adaptor dimers). The UMI was used to discard PCR duplicates and count single ligation events. Base calling was performed using CASAVA-1.8.2. The Illumina TruSeq index adaptor sequence was then trimmed when present by aligning its sequence, requiring a 100% match of the first five base pairs and a minimum global alignment score of 60 (Matches: 5, Mismatches: −4, Gap opening: −7, Gap extension: −7, Cost-free ends gaps). The UMI was clipped from the 5′ end and kept within the read name, for marking PCR duplicates. Reads were then depleted of rRNA, tRNA, snRNA, snoRNA and miscRNA, using Ensembl 80 annotations, as well as from RepeatMasker annotations, using strand-specific alignment with Bowtie2 v2.2.4 (Langmead and Salzberg, 2012). Next, reads were aligned to the *C. elegans* WBcel235 genome assembly using STAR version 2.4.2a (Dobin et al., 2013) with the following non-default parameters: *–alignEndsType EndToEnd–outFilterMultimapNmax 100–seedSearchStartLmax 15–sjdbScore 10–outSAMattributes All –limitBAMsortRAM 3221225472*. Genomic sequence indices for STAR were built including exon-junction coordinates from Ensembl 80. Finally, the STAR SJ.out.tab output files were parsed and the coverage of individual splice sites was compared between control and *rtcb-1(gk451)* (Table S1, "no neuronal injury" tab), and between *unc-70(s1502)* and *rtcb-1(gk451)*; *unc-70(s1502)* (Table S1, "neuronal injury" tab). For each comparison, we considered only splice sites i) were detected in at least two out three replicates of genotype 1, ii) were supported by at least three uniquely mapped reads in genotype 1 and iii) had a splice site coverage difference of at least 2-fold between the two genotypes after normalizing for changes in RNA abundance (Equation 1). A value of 0.01 was added to splice site coverages equal to 0 in genotype 2. Only uniquely mapped reads were considered in the calculation of splice site coverages and RPKM (Read Per Kilobase Million) values. Non-canonical splice site with > 10-fold difference in either of the two comparisons were annotated based on WormBase annotation (Table S2). Venn diagrams were drawn with Meta-chart.

$$\frac{\frac{ss\ coverage\ 1}{RPKM\ 1}}{\frac{ss\ coverage\ 2}{RPKM\ 2}} \qquad \text{(Equation 1)}$$

where *ss coverage 1* is the splice site coverage in genotype 1, *RPKM 1* is the mRNA's RPKM value in genotype 1, *ss coverage 2* is the splice site coverage in genotype 2, and *RPKM 2* is the mRNA's RPKM value in genotype 2.

Analysis of SHAPE-MaP data

Raw sequencing data were processed using the ShapeMapper pipeline (version 2.1.3) (Siegfried et al., 2014; Smola et al., 2015) with default parameters. SHAPE reactivities were only computed for nucleotides possessing sequencing depths above 1,000 in both modified and untreated samples. Nucleotides not passing this filter were treated as "no data" and excluded from downstream analysis. Secondary structure predictions and base pairing probabilities were generated using the SuperFold algorithm and SHAPE reactivities as restraints (Smola et al., 2015) with the following parameters: SHAPEintercept = −0.6, SHAPEslope = 1.8, trimInterior = 50, partitionWindowSize = 1200, PartitionStepSize = 100, foldWindowSize = 3000, foldStepSize = 300, maxPairingDist = 600.